Erschienen in: Solar Energy Materials and Solar Cells. Elsevier. 2023, 250, 112056
https://doi.org/10.1016/j.solmat.2022.112056

Influence of highly doped layers on hydrogen in-diffusion into crystalline silicon

Christian Fischer [a,*], Andreas Schmid [a], Axel Herguth [a], Annika Zuschlag [a], Pietro P. Altermatt [b], Phillip Hamer [c], Giso Hahn [a]

[a] *University of Konstanz, D-78457, Konstanz, Germany*
[b] *Trinasolar Co. Ltd, State Key Laboratory for Photovoltaic Science and Technology (SKL), Changzhou, 213031, Jiangsu Province, China*
[c] *School of Photovoltaic and Renewable Energy Engineering, The University of New South Wales, Kensington, NSW, 2052, Australia*

ARTICLE INFO

Keywords:
Highly doped layers
Hydrogen in-diffusion
Boron diffusion
Phosphorus diffusion
SIMS
Boron-hydrogen pairs

ABSTRACT

In this work, the influence of highly doped layers on the hydrogen in-diffusion into silicon from hydrogen-rich silicon nitride is investigated. Hydrogen in the crystalline silicon bulk of wafers with and without highly doped layers present was examined in solar cell-like structures by resistivity measurements for quantification of BH-pair dynamics. Hydrogen diffusion through phosphorus- and boron-doped Float-Zone samples without highly doped layers and with p^+- respectively n^+-layers was determined via secondary ion mass spectrometry. Therefore, deuterium concentration in an amorphous silicon layer on the backside was measured. This experiment shows an up to threefold increase of deuterium concentration in the amorphous layer for samples with highly doped layers present. A possible explanation of this observation is given by simulations.

1. Introduction

The role of hydrogen in silicon photovoltaics is quite ambivalent. On the one hand a sufficient hydrogenation effect is desired for bulk defect passivation, e.g. Refs. [1,2], increased surface passivation, e.g. Ref. [3], and in boron-doped Czochralski (Cz) material for regeneration of boron oxygen related light induced degradation (BO-LID) [4,5]. On the other hand, H is a very likely and commonly accepted component in light- and elevated temperature-induced degradation (LeTID), e.g. Refs. [6,7]. A correlation between hydrogen concentration [H] and the extent of LeTID was shown in Refs. [8,9].

Due to the versatile effects of hydrogen in crystalline Si (c-Si), a comprehensive understanding is required. Therefore, various efforts have been made in photovoltaic research in recent years. A good overview is provided by Hallam et al. [10].

One approach is controlling hydrogen concentration in c-Si. The H content present in the c-Si wafer can be influenced by various means, for example by adjusting H sources like H-rich silicon nitride (SiN_x:H) [11], by applying H barrier layers like AlO_x [9,12,13], or by adapted temperature treatments e.g., annealing steps [14].

Unfortunately, the detection and measurement of hydrogen in c-Si is quite sophisticated. Loss of hydrogen from sources like SiN_x:H due to a high temperature firing step can be determined via Fourier-transform infrared spectroscopy (FTIR), e.g. Ref. [15]. However, only a fraction diffuses into the c-Si bulk and the rest escapes to the atmosphere. The resulting hydrogen concentration in the c-Si bulk is in the range of 10^{14} to 10^{15} cm $^{-3}$ [16,17]. Those low concentrations are challenging for direct detection methods like e.g., secondary ion mass spectrometry (SIMS), as they are often limited by their background sensitivity [18]. An alternative for hydrogen detection in c-Si is via complex formation, whereby this only indicates the fraction involved in the formation. For example, formation of boron-hydrogen (BH) complexes results in an increase in resistivity due to deactivation of dopants and thus can be measured [17,19,20].

If solar cells are considered as a whole, there are not only passivating and H-rich layers on top of the c-Si bulk but also highly doped layers (HDL) like emitters or back and/or front surface fields. The influence of those HDL on hydrogen was investigated in various studies e.g., in Refs. [18,21,22]. For example, on p-type silicon an increased hydrogen passivation from H-rich plasma-enhanced chemical vapor deposited (PECVD) SiN_x:H in presence of an n^+-layer could be shown by Mittelstaedt et al. [23]. In n-type Cz silicon Chen et al. [7] showed the occurrence of LeTID, when highly doped layers were present during firing, which could be due to an increased H content. Additionally, a

* Corresponding author.
E-mail address: christian.fischer@uni-konstanz.de (C. Fischer).

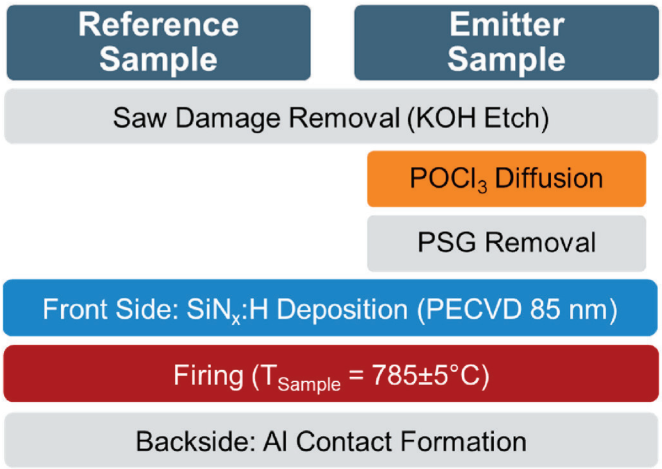

Fig. 1. Simplified process flow of BH-samples.

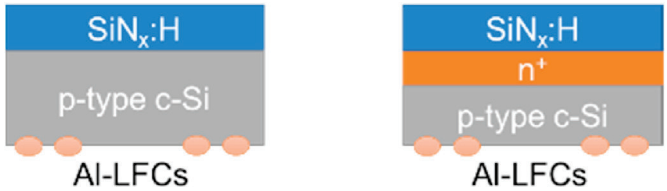

Fig. 2. Schematic reference sample (left) and emitter sample (right) structures for BH quantification, not to scale.

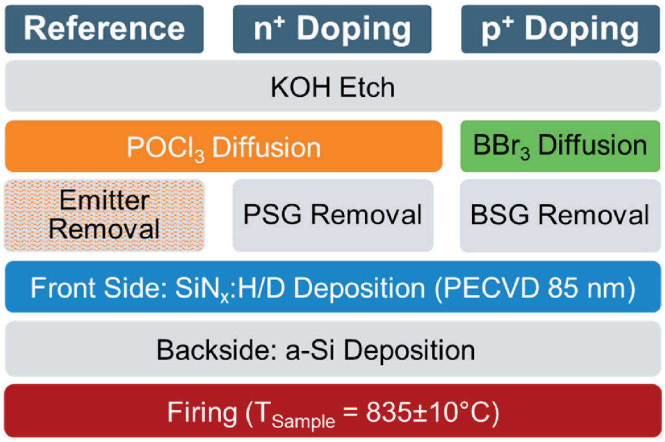

Fig. 3. Simplified process flow of samples for SIMS measurements.

model for hydrogen transport in c-Si solar cell structures from Hamer et al. [24] highlighted the significance of emitter layers and proposed a dependence of hydrogen diffusion through those layers on temperature and doping profiles.

Highly doped layers are present in most fabricated c-Si solar cells. Their influence on hydrogen diffusion is suggested by e.g., lifetime and degradation studies with presence of HDL [7,23]. However, only hydrogen correlated effects are reported. Therefore, in this paper, hydrogen diffusion from SiN_x:H layers in presence of HDL during firing is investigated. The formation of BH-pairs in c-Si wafers with or without HDL is detected via direct resistance measurements and thus the change in hydrogen dynamics in the bulk c-Si can be studied. In addition, boron- and phosphorus-doped FZ silicon is used and the concentration of deuterium, that is released from deuterated SiN_x:H/D diffusing through the c-Si wafer, is measured via SIMS in an amorphous silicon (a-Si) layer on the backside of the wafer. Simulations for hydrogen transport based on the model presented in Ref. [24] are performed and adapted to experimental results to give an insight on the possible distribution of hydrogen species in the samples and to assist in the explanation of the observed experimental findings.

2. Experimental

2.1. Sample preparation for BH quantification

Samples for quantification of BH pairs and their formation dynamics were prepared to investigate the influence of an emitter on hydrogen in-diffusion from SiN_x:H into the bulk. Samples with and without emitter layer are evaluated. The contacted resistance measurement was used as described by Winter and Herguth [25]. This method uses a four-terminal approach with aluminum laser fired contacts. The current required for measurement will thus not flow through the emitter.

The sample processing is shown in Fig. 1. Diamond wire-sawn FZ-Si wafers (~2.7 Ωcm p-type B-doped) were etched in potassium hydroxide (KOH) to a final thickness of 151 ± 10 μm to remove the saw damage. Samples were cleaned with a solution of ozonized deionized water and hydrochloric acid (HCl). After a dip in diluted hydrofluoric acid (HF) a second cleaning step for 10 min with piranha solution consisting of sulfuric acid (H_2SO_4) with hydrogen peroxide (H_2O_2) at 80 °C was performed. Finally, the wet-chemically grown silicon oxide was removed with another dip in diluted HF. One wafer received a single-sided phosphorus emitter (~50 Ω/sq) via back-to-back diffusion in a quartz tube furnace using $POCl_3$. The phosphorus silicate glass was removed with 10% HF and subsequently the wafer was cleaned again in the two-stage process described above (ozone + piranha). Afterwards, a single-sided H-rich SiN_x:H (~85 nm) was deposited with a direct plasma reactor (PlasmaLab 100, Oxford Instruments) and wafers were cut to 5 × 5 cm^2 samples. Both sample groups were fired in a Centrotherm belt furnace using a stand-off, with the temperature tracked (*DQ1860* from Datapaq in combination with a type-K thermocouple from Omega). Finally, all samples received via thermal evaporation deposited and laser fired Al contacts on the backside of the wafer for the contacted resistance measurement [25]. The resulting sample structures (shown in Fig. 2) were dark annealed at 220 °C to trigger BH pair formation.

In addition, a second group of BH samples with structure as shown in Fig. 2 left side was prepared to investigate the influence of the differing heating rates in the firing process for samples with emitter (cf. Fig. 7). Therefore, 1 Ωcm boron-doped FZ wafers were etched to 220 ± 10 μm thickness and cleaned as described above (material and thickness corresponds to the samples prepared for SIMS measurements). The firing profiles for those samples were adjusted to mimic both heating rates and peak temperatures of SIMS samples. Here, one BH sample corresponds to the temperature profile of the SIMS sample without emitter and the other BH sample corresponds to the temperature profile of the SIMS sample with emitter.

2.2. Sample preparation for SIMS

In principle SIMS allows direct measurement of hydrogen. However, typical H concentrations in the c-Si bulk are below the detection limit. Thus, a sample structure from Sheoran et al. is adapted [26] that uses H-lean sputtered a-Si on the rear side of the wafer as trapping layer for hydrogen and deuterium. The H/D is released from a SiN_x:H/D layer on the front side of the wafer and penetrates the silicon bulk during firing.

Two types of materials were investigated, 5 × 5 cm^2 boron- and phosphorus-doped (both ~1 Ωcm) FZ Si wafers with initial thickness of 250 μm. Three groups of samples were processed as shown in Fig. 3, resulting in a reference group with the highly doped layers removed before the penetration step, a group with n^+ and a group with p^+ layers. First, all wafers were KOH etched and subsequently cleaned in two steps with ozonized deionized water and piranha solution as described for the BH samples. Thereby the wafers from n^+ and p^+ groups were etched longer to compensate for the n^+-layer removal for the reference group

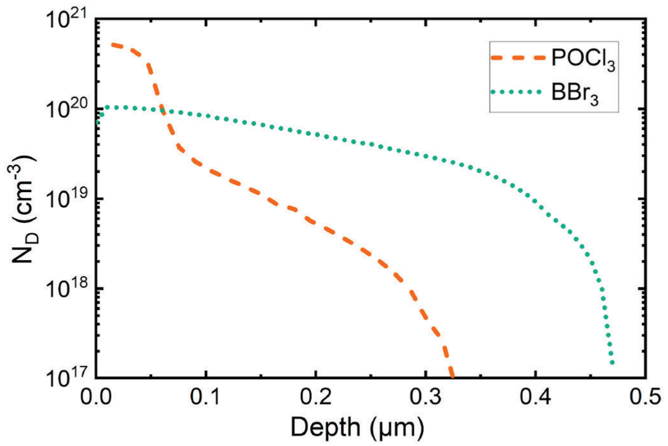

Fig. 4. Doping profiles from ECV measurement of P- and B-diffused samples.

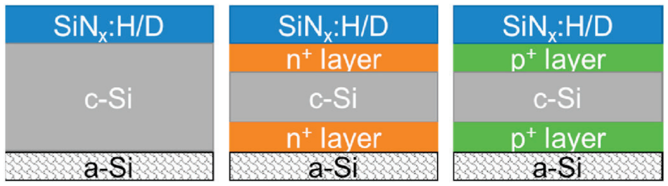

Fig. 5. Schematic sample structures for SIMS measurements of B- and P-doped c-Si wafers, not to scale.

after phosphorus-diffusion. Thus, all samples had a final thickness of 220 ± 10 μm after wet chemical processing.

Wafers from the reference group as well as the n^+ wafers were $POCl_3$ diffused (~50 Ω/sq), the p^+ wafers were BBr_3 diffused (~50 Ω/sq). Thus, highly B- or P-doped regions were formed on both sides of the respective wafer. For all diffusions electrically active dopant concentrations were determined via electrochemical capacitance-voltage (ECV) measurement and sheet resistivity was measured with the four-point probe technique. The doping profiles are shown in Fig. 4.

Boron and phosphorus silicate glasses were removed with 10% HF from all samples and the HDL were removed from reference samples. All wafers were wet chemically cleaned as previously described. Afterwards, 85 ± 5 nm of D-rich SiN_x:H/D was deposited on one side of the samples at 400 °C using a direct plasma reactor (PlasmaLab 100, Oxford Instruments) with deuterated ammonia (ND_3) and silane (SiH_4) as precursor. On the other side of the samples ~1 μm of almost H-free [27] amorphous Si was deposited (rf magnetron sputter device with a pure-Si target). The a-Si layer was applied without intentional heating and after SiN_x:H/D to prevent any heat induced D diffusion and contamination of a-Si with D during SiN_x:H/D deposition. The resulting sample structures are shown in Fig. 5. These structures allow to determine deuterium concentration [D] released from front side SiN_x:H/D diffusing through the c-Si wafer into the D-capturing a-Si-layer on the backside. For firing of samples, a belt furnace was used and furnace set parameters were adjusted to achieve comparable peak sample temperatures. Sample temperature was tracked with a *DQ1860* from Datapaq in combination with a type-K thermocouple from Omega pressed on the wafer, while the wafer was lying on a stand-off.

SIMS measurements of D profiles were performed from the backside through the a-Si-layer with a Cameca ims4f-E6 using a caesium primary ion beam.

3. Results and discussion

3.1. BH-quantification in samples with and without HDL

Hydrogen from the SiN_x:H layer is released during firing in a belt furnace and is quenched in the c-Si bulk with subsequent fast cooldown. According to Pritchard et al. [28] and the extended model of Voronkov and Falster [29], hydrogen introduced in this way is mainly present in dimer H_{2A} state and can form BH pairs at elevated temperature and thereby deactivate the dopant atoms during following annealing treatments. Finally, hydrogen will end in the speculated H_{2C} state and thus release dopant atoms again. In this work the analysis of changes in resistivity are performed as described by Herguth and Winter [20]. The data obtained from direct resistance measurements from samples treated for more than 200 h at 220 °C are shown in Fig. 6. Note that changes in resistance occurring during BH pair dynamics reflect only changes in BH pair concentration with respect to a reference point and not absolute concentrations. Under the assumption that long-term dissociation is almost complete, the change in BH pair concentration Δ[BH] is shown here with respect to the long-term limit of a double exponential approach as proposed in Ref. [20] being less sensitive to point-to-point variation.

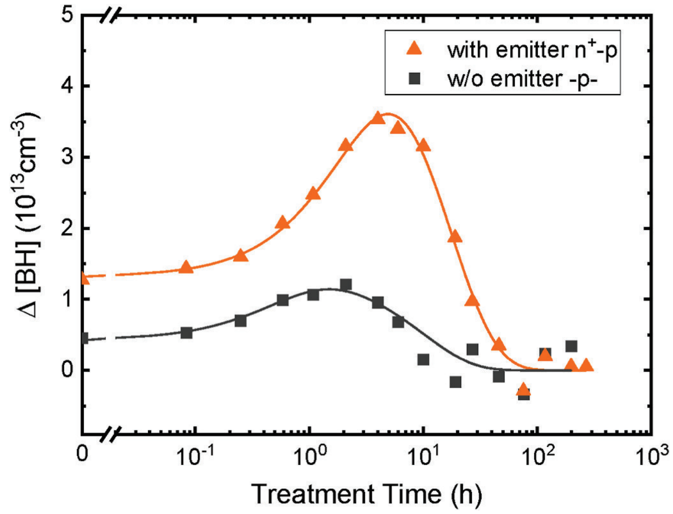

Fig. 6. Evolution and fits of the change in [BH] during dark annealing at 220 °C for samples with and without emitter.

When an n^+-layer was present during the firing process, there is a change in ΔBH-dynamics. Samples with HDL show increased maximum ΔBH. This could be an effect of different temporal evolution, as not only maximum Δ[BH] is changed, but also the temporal evolution. Differing

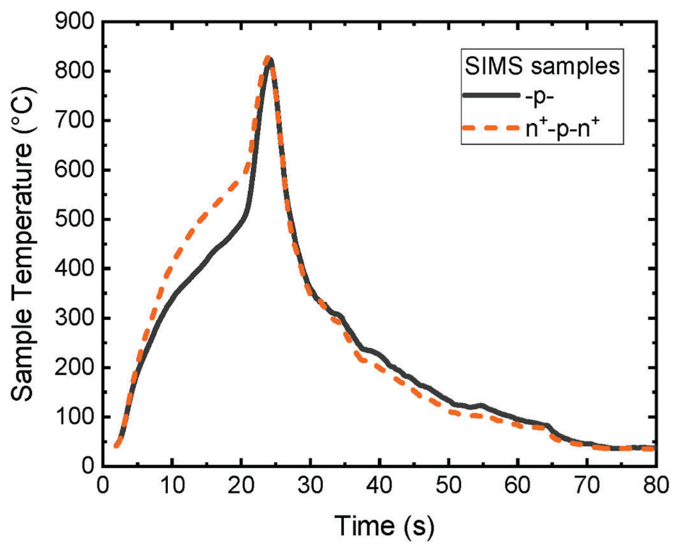

Fig. 7. Measured sample temperature in the fast-firing process of -p- and n^+-p-n^+ samples.

time constants for the samples with and without HDL are obtained in the fit with the double exponential approach shown in Fig. 6. If a direct influence of the SiN_x:H layer, which is identical in both samples, is ruled out, possible explanations for the changed dynamics have to consider the HDL. So the HDL can serve as hydrogen reservoir and release hydrogen during dark annealing into the c-Si bulk or it triggers an enhanced hydrogen diffusion from the SiN_x:H layer into the bulk c-Si during the firing process. Regarding the change in BH pair dissociation rate, the emitter layer could also hinder out-diffusion of hydrogen. Therefore, we conclude that the emitter layer actually influences hydrogen behavior in the c-Si bulk.

3.2. Role of firing profile on hydrogen in-diffusion

It is well known that the hydrogen release from SiN_x:H increases with firing temperature [4,30]. Therefore, in this work great attention was paid on similar peak firing temperatures, as samples with HDL heat up faster due to higher infrared absorption [31]. The tracked firing profiles of two exemplary samples, one with and one without HDL, used for SIMS measurements are given in Fig. 7. As can be seen, small variations in the heat-up phase below 600 °C remained. To check whether those variations during firing have a significant impact on hydrogen in-diffusion, two BH samples without HDL were used. One BH sample was fired according to the profile of the dotted line (similar to samples with emitter) and the other to match the solid line (similar to samples without emitter) in Fig. 7. Therefore, firing parameters had to be adjusted.

The H content introduced into the c-Si bulk during the different firing processes was again evaluated via measurement of BH pair dynamics. The results shown in Fig. 8 were again fitted with a double-exponential approach and use the long-term limit of the fit function as reference point, as described above for Fig. 6. (Note that maximum Δ[BH] between those two figures cannot be compared, as base material and peak temperature are not comparable.) The samples without emitter layer but adjusted firing profiles show no significant difference regarding kinetics and maximum Δ[BH] even though the temperature profiles differ during the heat-up phase below 600 °C. This is not too surprising because hydrogen release from SiN_x:H layers occurs mainly at temperatures above 650 °C, e.g. Ref. [4] and the vanishing extent of (hydrogen-related) LeTID below 650 °C [32] suggests a negligible hydrogen in-diffusion from SiN_x:H layers especially below 600 °C. Hence the observed variation during the heat-up phase in Fig. 7 seems to be tolerable.

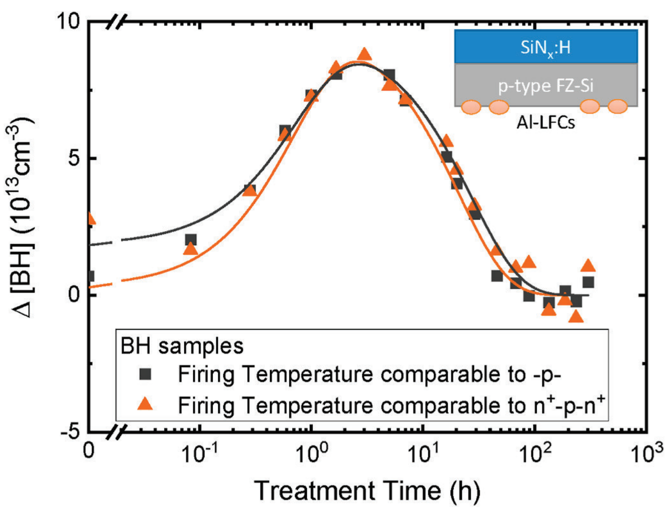

Fig. 8. Evolution and fits of the change in [BH] during dark annealing at 220 °C for samples with adapted temperature profiles as shown in Fig. 7. The inlay shows the sample structure.

Table 1
Fast firing set peak and peak sample temperatures.

Sample structure	-p-	n^+-p-n^+	p^+-p-p^+	-n-	n^+-n-n^+	p^+-n-p^+
Set peak temperature (°C)	900	865	865	940	870	870
Sample peak temperature (°C)	824	829	831	844	835	837

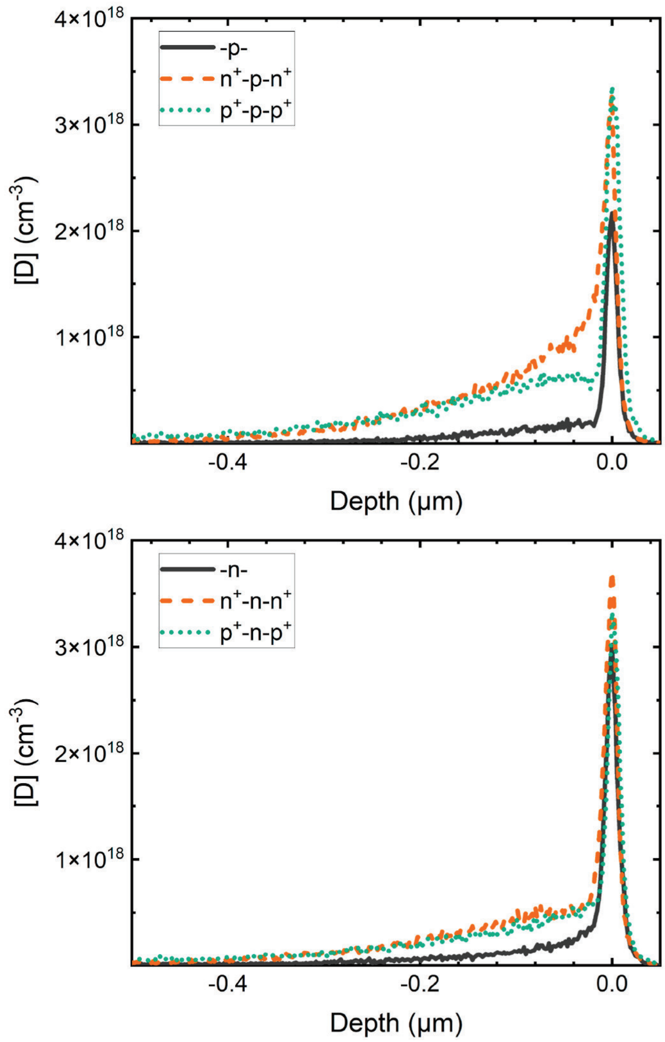

Fig. 9. Observed deuterium concentration dependent on SIMS sputter depth for p- and n-type samples with base material without or with highly doped layers (n^+ and p^+). B-doped base material (top). P-doped base material (bottom).

3.3. Hydrogen diffusion through HDL

In this work, SIMS is used for quantification of deuterium diffusion through highly doped layers. However, a direct detection within the bulk c-Si is not possible. Therefore, an a-Si layer for trapping of deuterium on the wafer backside was used, as demonstrated in previous studies. For example, Sheoran et al. could show an increased deuterium in-diffusion from SiN_x:H for prolonged annealing times at 750 °C [26], and Schmid et al. investigated the H-blocking capability of AlO_x--interlayers by SIMS [9], both using SIMS for detection of deuterium in the a-Si layer. However, this was after exposure to deuterium plasma for longer times at low temperatures (6 h 120 °C and 6 h 105 °C), which leads to increased dopant-hydrogen pair formation [33]. Nevertheless, to measure possible elevated deuterium concentrations in the HDL, a

Table 2
Deuterium content in a-Si (integrated from −0.5 to 0.05 μm).

Sample structure	*-p-*	*n^+-p- n^+*	*p^+-p-p^+*	*-n-*	*n^+-n- n^+*	*p^+-n-p^+*
Deuterium (10^{12} cm^{-2})	6.1	21.6	20.0	8.6	17.0	15.7

symmetrical sample structure was used with HDL on both sides of the c-Si bulk. On the front side the highly doped layer can influence hydrogen/deuterium introduction into the c-Si wafer and on the backside it is used to potentially trap deuterium in this layer for the SIMS measurement. Of course, the layer on the backside could also influence hydrogen/deuterium diffusion.

As previously discussed, it was essential to adapt the set firing temperature. The measured sample temperatures and the corresponding firing set peak temperatures of the SIMS samples are given in Table 1. Set peak temperature was reduced for the samples with HDL, so that the wafer temperature of all investigated samples is comparable. The variation within a material group was <10 °C and over all <20 °C.

SIMS data show measurable amounts of D (>10^{15} cm^{-3}) in the a-Si layer with highest concentrations in the range of 10^{18} cm^{-3}. The data for p-type samples are given in Fig. 9 (top) and the data for n-type sample in Fig. 9 (bottom). Deuterium released from the SiN_x:H/D layer on the front side diffuses through the wafer during firing and is trapped in the a-Si-layer. Therefore, the highest D concentrations are observed at the a-Si/c-Si interface Si and the given sputtering depth relates to this position to compensate for potential sample-to-sample thickness variations of the a-Si layer. As all samples show a similar strong drop towards the HDL, respectively the Si bulk, and the D signal falls below the detection limit in less than 50 nm, the HDL does not seem to contain significant amounts of trapped D above the detection limit (10^{15} cm^{-3}). It is even likely that the observed decrease in the c-Si is at least partly a measurement artifact as light elements as D tend to be pushed into the substrate by the bombardment with heavy Cs ions and that [D] at the interface is likely even more abrupt.

Since the peak values usually result from only one or two measurement points and are thus subject to uncertainty, an integral in depth was used to compare the amount of D in the a-Si. This reduces the influence of non-systematic errors. Nevertheless, the integrated values usually show the same tendency as the peak values. In addition, integrated D concentration better accounts for the amount of deuterium diffused through the sample. The integrated [D] was calculated from −0.5 μm to 0.05 μm depth (Table 2). In this area, concentration increases on both sides of the peak from below detection limit towards the peak value at the a-Si interface (located at 0 μm). As the observed [D] depth profiles extend only over a part of the total a-Si thickness of 1 μm, unwanted D in-diffusion from the ambient can be excluded.

The deuterium content measured in the a-Si layer on the backside was released from the front side SiN_x:H/D and diffuses through the wafer during the firing step. For p-type bulk material the integrated D content in the a-Si is more than threefold higher with both types of HDL present during the firing step. Samples with HDL (p^+- respectively n^+-layers) show increased area integrated deuterium concentrations and the difference between highly P-doped layers compared to highly B-doped layers is rather small. This also holds true for n-type base material. However, in n-type material the difference between samples with and without HDL is only twofold.

An increased area integrated deuterium concentration in the a-Si layer after firing is observed with HDL (p^+- respectively n^+-layers). Therefore, it can be speculated that the doping concentration of the HDL impacts the observed deuterium concentration. This could also explain the higher area integrated deuterium concentration in the a-Si for n^+-compared to p^+-layers, as peak doping concentrations for n^+-layers are higher at the c-Si/SiN_x:H interface (cf. Fig. 4).

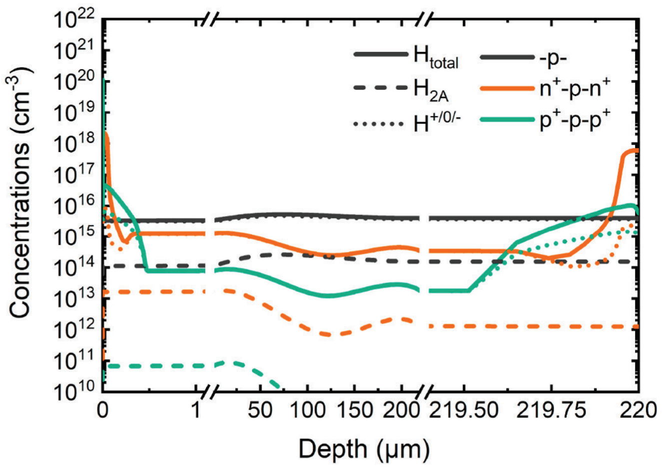

Fig. 10. Simulated concentration of hydrogen species, which are injected from the SiN_x:H layer at the left and diffuse towards the right, into the a-Si layer on the other side of the wafer. Standard segregation coefficient of H between SiN_x:H and c-Si was used for all samples.

3.4. Simulation of hydrogen diffusion

To clarify the reasons for the observed behavior and to give an insight into the possible distribution of the hydrogen species in the c-Si bulk, the hydrogen diffusion was simulated numerically with Sentaurus Process [34]. An updated version of the model described in Ref. [24] was used. The doping profiles in Fig. 4 and the firing profiles in Fig. 7 serve as input. The simulations show the hydrogen species at a temperature of 700 °C during the cooling process (1.5s after peak temperature). At this temperature mobile interstitial hydrogen atoms ($H^{+/0/-}$) are still the dominant species and the vast majority of hydrogen transport across the c-Si/SiN_x:H interface has already taken place. The mobile hydrogen reaching the backside during cooldown is collected by the a-Si-layer on the backside of the sample in the experiment. Therefore, simulations show these mobile hydrogen states during cooldown, as those are the species contributing to the concentration in the a-Si-layer. However, total concentrations of SIMS and simulations do not match, as simulations show only the state for one temperature and the a-Si-layer is collecting all mobile hydrogen reaching the backside during complete cooldown from peak firing temperature to room temperature.

In Fig. 10 the simulated concentrations of total hydrogen, the mobile interstitial species and hydrogen dimers (H_{2A}) are shown for all three sample types with a boron base-doping. There are two key observations. Firstly, while the total hydrogen concentration at the rear surface is higher for diffused samples, the interstitial hydrogen concentration is not. This is because the majority of hydrogen in the diffused region is paired with dopants. Secondly, the concentration of the interstitial mobile hydrogen is lower in the bulk for the diffused samples than for the undiffused samples.

These simulation results are in clear contradiction to the experimental data, which provides strong evidence of increased hydrogen concentrations in both the bulk and at the rear surface for diffused samples. The disagreement at the rear surface might be resolved through altering the parameters for hydrogen-dopant pairing, such that a greater proportion of the total hydrogen at this surface is in the interstitial state. However, this would still result in a lower bulk concentration for diffused samples compared to undiffused ones.

One possible explanation is that more hydrogen is transported across the c-Si/SiN_x:H interface in the presence of a diffused layer. Fig. 11 presents simulations performed with increased in-diffusion of hydrogen for diffused surfaces. In the current model this was achieved through increasing the segregation coefficient at the interface for the samples with HDL (higher segregation coefficient not used for the sample

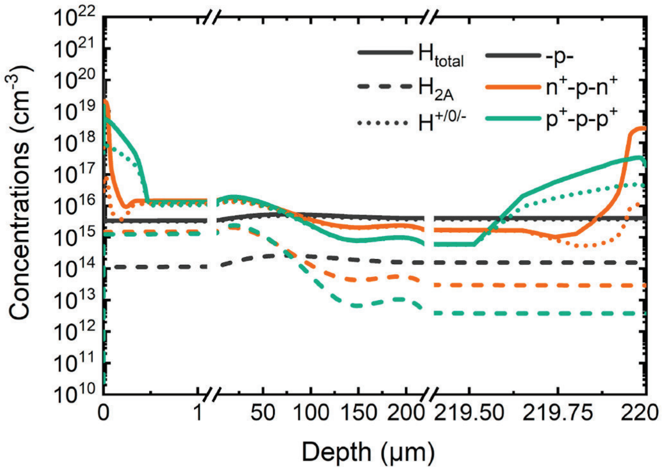

Fig. 11. Simulated concentration of hydrogen species, which are injected from the SiN_x:H layer at the left and diffuse towards the right, into the a-Si layer on the other side of the wafer. Standard segregation coefficient of H between SiN_x:H and c-Si was used for the un-diffused sample (-p-). An adapted segregation coefficient for higher H in-diffusion was used for the diffused sample (n^+-p-n^+ and p^+-p-p^+).

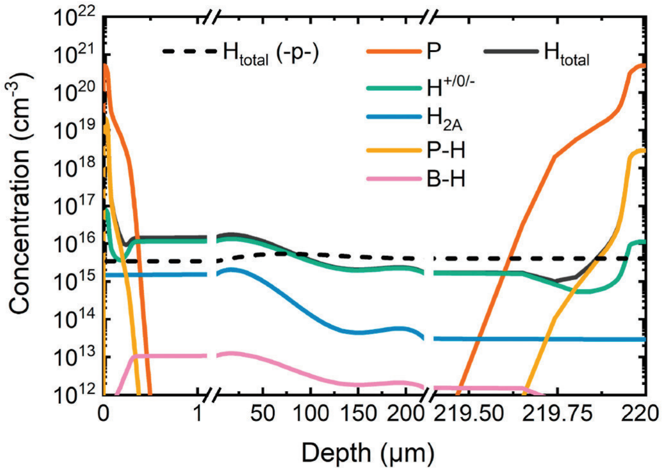

Fig. 12. Simulated concentration of hydrogen species, which are injected from the SiN_x:H layer at the left and diffuse towards the right, into the a-Si layer on the other side of the wafer. Concentrations are given for an n^+-p-n^+ sample structure with adapted segregation coefficient for H. Total [H] in sample with HDL using adapted segregation coefficient (black solid line) and in reference sample without HDL using standard segregation coefficient (black dashed line).

without HDL), although similar results could be achieved through changes in other parameters.

Simulations with adapted segregation coefficient for samples with HDL are in a significantly better agreement with experimental data. The concentrations for mobile hydrogen species are significantly higher at the backside for the diffused samples (n^+-p-n^+ and p^+-p-p^+). This supports the hypothesis that HDL increase H in-diffusion. This could possibly be due to surface disturbances caused by HDL formation. An overview of all hydrogen species for the phosphorus-diffused sample and a comparison of total H content with the undiffused sample is given in Fig. 12. Most of the hydrogen is in H^+ state, except within phosphorus doped layers where hydrogen is negatively charged. During further cooldown dimers H_{2A} and BH- respectively PH-pairs are formed and the concentration of $H^{+/0/-}$ decreases.

4. Conclusion

In general, it was observed that during the firing processes, the presence of a highly doped layer does not hinder H in-diffusion from H-rich layers. In fact, it could be shown that [H] in the c-Si bulk is probably increased by the presence of these layers (for p^+- and n^+-type doping). ΔBH data indicate that the emitter layer influences hydrogen behavior in the c-Si bulk. Based on simulation results and SIMS data the most likely explanation for the increased ΔBH is an increased hydrogen concentration in the bulk. Thereby, it was confirmed that an emitter on p-type wafer increases hydrogenation. In addition, this was also observed on n-type material with highly doped layers present by SIMS. The increased in-diffusion of H observed for samples with highly doped layers could possibly be explained by a surface damage caused by formation of layers with high dopant concentrations. Therefore, considering degradation studies solely performed on lifetime sample structures (without highly doped layers) could tend to underestimate degradation phenomena related to H in solar cells.

CRediT authorship contribution statement

Christian Fischer: Writing – review & editing, Writing – original draft, Visualization, Methodology, Investigation, Conceptualization. **Andreas Schmid:** Writing – review & editing, Methodology, Conceptualization. **Axel Herguth:** Writing – review & editing, Validation, Supervision, Formal analysis, Conceptualization. **Annika Zuschlag:** Writing – review & editing, Supervision, Conceptualization. **Pietro P. Altermatt:** Writing – original draft, Visualization, Software, Formal analysis. **Phillip Hamer:** Writing – review & editing, Software, Methodology, Data curation. **Giso Hahn:** Writing – review & editing, Supervision, Project administration, Funding acquisition, Conceptualization.

Declaration of competing interest

The authors declare that they have no known competing financial interests or personal relationships that could have appeared to influence the work reported in this paper.

Data availability

Data will be made available on request.

Acknowledgements

The authors would like to thank all helping hands in the group. Part of this work was financially supported by the German Federal Ministry for Economic Affairs and Climate Action (FKZ 03EE1052A, HYDRA). The content is the responsibility of the authors.

References

[1] R. Luedemann, Hydrogen passivation of multicrystalline silicon solar cells, Mater. Sci. Eng.: B 58 (1-2) (1999) 86–90. https://doi:10.1016/s0921-5107(98)00288-8.
[2] B. Hallam, D. Chen, M. Kim, B. Stefani, B. Hoex, M. Abbott, S. Wenham, The role of hydrogenation and gettering in enhancing the efficiency of next-generation Si solar cells: an industrial perspective, Phys. Status Solidi 214 (7) (2017), 1700305. https://doi:10.1002/pssa.201700305.
[3] R.S. Bonilla, B. Hoex, P. Hamer, P.R. Wilshaw, Dielectric surface passivation for silicon solar cells: a review, Phys. Status Solidi 214 (7) (2017), 1700293. https://doi:10.1002/pssa.201700293.
[4] S. Wilking, S. Ebert, A. Herguth, G. Hahn, Influence of hydrogen effusion from hydrogenated silicon nitride layers on the regeneration of boron-oxygen related defects in crystalline silicon, J. Appl. Phys. 114 (19) (2013), 194512. https://doi:10.1063/1.4833243.
[5] L. Helmich, D.C. Walter, R. Falster, V.V. Voronkov, J. Schmidt, Impact of hydrogen on the boron-oxygen-related lifetime degradation and regeneration kinetics in crystalline silicon, Sol. Energy Mater. Sol. Cells 232 (2021), 111340. https://doi:10.1016/j.solmat.2021.111340.

[6] T. Niewelt, F. Schindler, W. Kwapil, R. Eberle, J. Schön, M.C. Schubert, Understanding the light-induced degradation at elevated temperatures: similarities between multicrystalline and floatzone p-type silicon, Prog. Photovoltaics Res. Appl. 26 (8) (2017) 533–542. https://doi:10.1002/pip.2954.
[7] D. Chen, P.G. Hamer, M. Kim, T.H. Fung, G. Bourret-Sicotte, S. Liu, C.E. Chan, A. Ciesla, R. Chen, M.D. Abbott, B.J. Hallam, S.R. Wenham, Hydrogen induced degradation: a possible mechanism for light- and elevated temperature- induced degradation in n-type silicon, Sol. Energy Mater. Sol. Cells 185 (2018) 174–182. https://doi:10.1016/j.solmat.2018.05.034.
[8] J. Schmidt, D. Bredemeier, D.C. Walter, On the defect physics behind light and elevated temperature-induced degradation (LeTID) of multicrystalline silicon solar cells, IEEE J. Photovoltaics 9 (6) (2019) 1497–1503. https://doi:10.1109/jphotov.2019.2937223.
[9] A. Schmid, C. Fischer, D. Skorka, A. Herguth, C. Winter, A. Zuschlag, G. Hahn, On the role of AlO_x thickness in AlO_x/SiN_y: H layer stacks regarding light- and elevated temperature-induced degradation and hydrogen diffusion in c-Si, IEEE J. Photovoltaics 11 (4) (2021) 967–973. https://doi:10.1109/jphotov.2021.3075850.
[10] B.J. Hallam, P.G. Hamer, A.M.C. ńee Wenham, C.E. Chan, B.V. Stefani, S. Wenham, Development of advanced hydrogenation processes for silicon solar cells via an improved understanding of the behaviour of hydrogen in silicon, Prog. Photovoltaics Res. Appl. 28 (2020) 1217–1238. https://doi:10.1002/pip.3240.2.
[11] J.-F. Lelièvre, E. Fourmond, A. Kaminski, O. Palais, D. Ballutaud, M. Lemiti, Study of the composition of hydrogenated silicon nitride SiN_x:H for efficient surface and bulk passivation of silicon, Sol. Energy Mater. Sol. Cells 93 (8) (2009) 1281–1289. https://doi:10.1016/j.solmat.2009.01.023.
[12] L. Helmich, D.C. Walter, D. Bredemeier, J. Schmidt, Atomic-layer-deposited Al_2O_3 as effective barrier against the diffusion of hydrogen from SiN_x :H layers into crystalline silicon during rapid thermal annealing, Phys. Status Solidi Rapid Res. Lett. (2020), 2000367. https://doi:10.1002/pssr.202000367.
[13] U. Varshney, B. Hallam, P. Hamer, A. Ciesla, D. Chen, S. Liu, C. Sen, A. Samadi, M. Abbott, C. Chan, B. Hoex, Controlling light- and elevated-temperature-induced degradation with thin film barrier layers, IEEE J. Photovoltaics 10 (1) (2020) 19–27. https://doi:10.1109/jphotov.2019.2945199.
[14] C. Boehme, G. Lucovsky, H loss mechanism during anneal of silicon nitride: chemical dissociation, J. Appl. Phys. 88 (10) (2000) 6055–6059. https://doi:10.1063/1.1321730.
[15] P.S. Peercy, H.J. Stein, B.L. Doyle, S.T. Picraux, S. Laboratoriest, Hydrogen concentration profiles and chemical bonding in silicon nitride, J. Electron. Mater. 8 (1) (1979) 11–24. https://doi:10.1007/bf02655637.
[16] G. Hahn, D. Karg, A. Schonecker, A. Burgers, R. Ginige, K. Cherkaoui, Kinetics of hydrogenation and interaction with oxygen in crystalline silicon, in: Conf. Rec. Of the 31st, IEEE Photovolt. Specialists Conf., 2005, pp. 1035–1038. https://doi:10.1109/PVSC.2005.1488310.
[17] D.C. Walter, D. Bredemeier, R. Falster, V.V. Voronkov, J. Schmidt, Easy-to-apply methodology to measure the hydrogen concentration in boron-doped crystalline silicon, Sol. Energy Mater. Sol. Cells 200 (2019), 109970. https://doi:10.1016/j.solmat.2019.109970.
[18] S. Pearton, Diffusion of hydrogen in n-type Si, Mater. Sci. Eng.: B 23 (2) (1994) 130–136. https://doi:10.1016/0921-5107(94)90346-8.
[19] A.J. Tavendale, D. Alexiev, A.A. Williams, Field drift of the hydrogen-related, acceptor-neutralizing defect in diodes from hydrogenated silicon, Appl. Phys. Lett. 47 (3) (1985) 316–318. https://doi:10.1063/1.96204.
[20] A. Herguth, C. Winter, Methodology and error analysis of direct resistance measurements used for the quantification of boron–hydrogen pairs in crystalline silicon, IEEE J. Photovoltaics 11 (4) (2021) 1059–1068. https://doi:10.1109/jphotov.2021.3074463.
[21] P.I. Widenborg, A.G. Aberle, Hydrogen-induced dopant neutralisation in p-type AIC poly-si seed layers functioning as buried emitters in ALICE thin-film solar cells on glass, J. Cryst. Growth 306 (1) (2007) 177–186. https://doi:10.1016/j.jcrysgro.2007.03.053.
[22] S. Shumate, M.G. Young, H.M. Khaja, D. Hutchings, L. Cousar, S.-Q. Yu, H. Naseem, Progress on the hydrogen selective emitter for n-type solar cells, in: 2013 IEEE 39th Photovolt. Specialists Conf. (PVSC), IEEE, 2013. https://doi:10.1109/pvsc.2013.6744931.
[23] L. Mittelstaedt, A. Metz, R. Hezel, Hydrogen passivation of defects in EFG ribbon silicon, Sol. Energy Mater. Sol. Cells 72 (1-4) (2002) 255–261. https://doi:10.1016/s0927-0248(01)00172-6.
[24] P. Hamer, B. Hallam, R.S. Bonilla, P.P. Altermatt, P. Wilshaw, S. Wenham, Modelling of hydrogen transport in silicon solar cell structures under equilibrium conditions, J. Appl. Phys. 123 (4) (2018), 043108. https://doi:10.1063/1.5016854.
[25] C. Winter, A. Herguth, Contacted resistance measurements for the quantification of boron-hydrogen pairs in crystalline silicon, AIP Conf. Proc. 2487 (1) (2022) 130016-1–130016-7, https://doi.org/10.1063/5.0089294.
[26] M. Sheoran, D.S. Kim, A. Rohatgi, H.F.W. Dekkers, G. Beaucarne, M. Young, S. Asher, Hydrogen diffusion in silicon from plasma-enhanced chemical vapor deposited silicon nitride film at high temperature, Appl. Phys. Lett. 92 (17) (2008), 172107. https://doi:10.1063/1.2917467.
[27] S. Gerke, G. Hahn, R. Job, B. Terheiden, Bias-plasma assisted RF magnetron sputter deposition of hydrogen-less amorphous silicon, Energy Proc. 84 (2015) 105–109. https://doi:10.1016/j.egypro.2015.12.302.
[28] R.E. Pritchard, J.H. Tucker, R.C. Newman, E.C. Lightowlers, Hydrogen molecules in boron-doped crystalline silicon, Semicond. Sci. Technol. 14 (1) (1999) 77–80. https://doi:10.1088/0268-1242/14/1/011.
[29] V.V. Voronkov, R. Falster, Formation, dissociation, and diffusion of various hydrogen dimers in silicon, Phys. Status Solidi 254 (6) (2017), 1600779. https://doi:10.1002/pssb.201600779.
[30] C. Boehme, G. Lucovsky, Dissociation reactions of hydrogen in remote plasma-enhanced chemical-vapor-deposition silicon nitride, J. Vac. Sci. Technol.: Vac., Surf., and Films 19 (5) (2001) 2622–2628. https://doi:10.1116/1.1398538.
[31] W. Spitzer, H.Y. Fan, Infrared absorption in n-type silicon, Phys. Rev. 108 (2) (1957) 268–271. https://doi:10.1103/physrev.108.268.
[32] C. Vargas, K. Kim, G. Coletti, D. Payne, C. Chan, S. Wenham, Z. Hameiri, Influence of silicon nitride and its hydrogen content of carrier-induced degradation in multicrystalline silicon, in: Proc. 33rd Eur. Photovolt. Sol. Energy Conf. Exhib. Amsterdam, 2017, pp. 561–564. https://10.4229/EUPVSEC20172017-2AV.1.38.
[33] M. Binns, R. Newman, S. McQuaid, E.C. Lightowlers, Hydrogen solubility and defects in silicon, Mater, Sci. Forum 143–147 (1993) 861–866. https://doi:10.4028/www.scientific.net/msf.143-147.861.
[34] Sentaurus Process, Manual 2022, Synopsys, Mountain View, CA.